Eur. Phys. J. B **84**, 255–264 (2011)
DOI: 10.1140/epjb/e2011-20384-6

THE EUROPEAN PHYSICAL JOURNAL B

Regular Article

Electronic structure of disclinated graphene in a uniform magnetic field

J. Smotlacha[1], R. Pincak[2,3,a], and M. Pudlak[3]

[1] Faculty of Nuclear Sciences and Physical Engineering, Czech Technical University, Brehova 7, 11000 Prague, Czech Republic
[2] Bogoliubov Laboratory of Theoretical Physics, Joint Institute for Nuclear Research, 141980 Dubna, Moscow region, Russia
[3] Institute of Experimental Physics, Slovak Academy of Sciences, Watsonova 4704353 Kosice, Slovak Republic

Received 19 May 2011 / Received in final form 15 August 2011
Published online 10 November 2011 –

Abstract. The electronic structure in the vicinity of the 1-heptagonal and 1-pentagonal defects in the carbon graphene plane is investigated for the case of hyperboloidal geometry. Using a continuum gauge field-theory model, the local density of states around the Fermi energy is calculated for both cases. In this model, the disclination is represented by a SO(2) gauge vortex and the corresponding metrics follows from the elasticity properties of the graphene membrane. To enhance the interval of energies, a self-consistent perturbation scheme is used. The Landau states are investigated and compared with the predicted values. A discussion on the influence of the Zeeman effect is included.

1 Introduction

Nanostructured carbon materials are materials with a special geometrical structure of their molecules which we call carbon nanoparticles. This geometrical structure is accompanied by the topological defects in a hexagonal planar lattice called graphene.

There are many variously-shaped carbon nanostructures known. The most famous is fullerene, which has the structure of a soccer ball and can be approximated as a sphere. It is composed of 60 carbon atoms which create 20 hexagons and 12 pentagons [1,2]. However other structures also exist, for example nanocones, nanotoroids, nanotubes, nanohorns etc. A wide variety of electronic properties of these structures have been studied. Some of these properties are given by magnetic properties [3,4], optical absorption spectra or electronic properties of nanotube caps [5]. They suggest a potential use in nanoscale devices like quantum wires, nonlinear electronic elements, transistors, molecular memory devices or electron field emitters. From a theoretical point of view, it was predicted and experimentally verified by scanning tunneling microscopy that metallic or semiconducting properties of carbon nanotubes depend on whether or not the difference $n - m$ of the components of the chiral vector (n, m) is a multiple of 3 [6–8].

In most cases, the defects in graphene originate from the presence of the pentagons for the positive curvature and the heptagons for the negative curvature [9]. More complicated structures can arise when two variously-shaped parts of nanoparticles are connected by a region with pentagon-heptagon pairs. It seems that the best approximation for pentagonal and heptagonal areas is hyperboloid – positively curved for pentagons and negatively curved for heptagons [10].

The electronic properties of these structures can be explored by solving the Dirac equation at a curved surface [11]. In this paper, after introducing the computational formalism, some geometrical properties of the defects are investigated. After doing this, we study the Gaussian curvature of the surface. With the help of the Dirac equation, the local density of states (LDoS) for disclinated areas near the Fermi level (close to the zero energy) is then calculated for both pentagonal and heptagonal defects. It will be influenced by a uniform magnetic field. Then we compare the electronic properties of both the models and, finally, we examine the corresponding Landau states, the influence of the Zeeman effect on them and compare them with the approximate formulae from earlier works. The model described in [10] is used. In this model, the aforementioned hyperboloidal geometry is considered.

2 Basic formalism

First, we introduce the Dirac equation in $(2 + 1)$ dimensions. It has the form:

$$i\gamma^{\alpha} e_{\alpha}^{\mu} [\nabla_{\mu} - ia_{\mu} - iA_{\mu}]\psi = E\psi. \tag{1}$$

The wave function ψ, the so-called bispinor, is composed of two parts:

$$\psi = \begin{pmatrix} \psi_A \\ \psi_B \end{pmatrix}, \tag{2}$$

[a] e-mail: pincak@saske.sk

each corresponding to different sublattices of the curved graphene sheet. The gauge field $a_\mu, \mu = \xi, \varphi$ arises from spin rotation invariance for atoms of different sublattices A and B in the Brillouin zone [12].

The zweibein e_α stands for incorporating fermions on the curved 2D surface and it has to yield the same values of observed quantities for different choices related by the local SO(2) rotations:

$$e_\alpha \to e'_\alpha = \Lambda^\beta_\alpha e_\beta, \qquad \Lambda^\beta_\alpha \in SO(2). \tag{3}$$

For this purpose, a covariantly-constant local gauge field ω_μ is incorporated [13]:

$$\partial_\mu e^\alpha_\nu - \Gamma^\rho_{\mu\nu} e^\alpha_\rho + (\omega_\mu)^\alpha_\beta e^\beta_\nu = 0, \tag{4}$$

where Γ_μ is the Levi-Civita connection coming from the metrics $g_{\mu\nu}$ (see below). Then ω_μ is called the spin connection. Next, the covariant derivative ∇_μ is defined as:

$$\nabla_\mu = \partial_\mu + \Omega_\mu, \tag{5}$$

where

$$\Omega_\mu = \frac{1}{8}\omega^{\alpha\beta}_\mu [\gamma_\alpha, \gamma_\beta] \tag{6}$$

denotes the spin connection in the spinor representation. The Dirac matrices γ_α can be replaced in two dimensions by the Pauli matrices σ_α:

$$\gamma_1 = -\sigma_2, \qquad \gamma_2 = \sigma_1. \tag{7}$$

A_μ is the vector potential arising from the external magnetic field.

The metric $g_{\mu\nu}$ of the 2D surface comes from following parametrisation, with the help of two parameters ξ, φ:

$$(\xi, \varphi) \to \overrightarrow{R} = (x(\xi, \varphi), y(\xi, \varphi), z(\xi, \varphi)), \tag{8}$$

where

$$0 \le \xi < \infty, \qquad 0 \le \varphi < 2\pi. \tag{9}$$

The 4 components of the metric are defined as:

$$g_{\mu\nu} = \partial_\mu \overrightarrow{R} \partial_\nu \overrightarrow{R}. \tag{10}$$

The hyperboloid geometry which we use has, for both heptagons and pentagons, very similar but not identical parametrisation. We consider it in separate chapters. Generally, the non-diagonal components of the metric are:

$$g_{\xi\varphi} = g_{\varphi\xi} = 0. \tag{11}$$

For the zweibeins and the diagonal components of the metric the following relationships hold:

$$e^1_\xi = \sqrt{g_{\xi\xi}} \cos\varphi, \qquad e^1_\varphi = -\sqrt{g_{\varphi\varphi}} \sin\varphi, \tag{12}$$

$$e^2_\xi = \sqrt{g_{\xi\xi}} \sin\varphi, \qquad e^2_\varphi = \sqrt{g_{\varphi\varphi}} \cos\varphi, \tag{13}$$

and for the spin connection coefficients ω_μ:

$$de^1 = -\omega^{12} \wedge e^2, \qquad de^2 = -\omega^{21} \wedge e^1, \qquad \omega^{12} = -\omega^{21}, \tag{14}$$

so:

$$\omega^{12}_\varphi = -\omega^{21}_\varphi = 1 - \frac{\partial_\xi \sqrt{g_{\varphi\varphi}}}{\sqrt{g_{\xi\xi}}} = 2\omega, \tag{15}$$

$$\omega^{12}_\xi = \omega^{21}_\xi = 0. \tag{16}$$

Then the coefficients Ω_μ are:

$$\Omega_\xi = 0, \qquad \Omega_\varphi = i\omega\sigma_3. \tag{17}$$

If we write the wave function in the form

$$\begin{pmatrix} \psi_A \\ \psi_B \end{pmatrix} = \frac{1}{\sqrt[4]{g_{\varphi\varphi}}} \begin{pmatrix} \widetilde{u}(\xi) e^{i\varphi j} \\ \widetilde{v}(\xi) e^{i\varphi(j+1)} \end{pmatrix}, \qquad j = 0, \pm 1, \ldots \tag{18}$$

and substituting (18) into (1) we obtain

$$\partial_\xi \widetilde{u} - (j + 1/2 - a_\varphi + A_\varphi) \sqrt{\frac{g_{\xi\xi}}{g_{\varphi\varphi}}} \widetilde{u} = E \sqrt{g_{\xi\xi}} \widetilde{v}, \tag{19}$$

$$-\partial_\xi \widetilde{v} - (j + 1/2 - a_\varphi + A_\varphi) \sqrt{\frac{g_{\xi\xi}}{g_{\varphi\varphi}}} \widetilde{v} = E \sqrt{g_{\xi\xi}} \widetilde{u}. \tag{20}$$

3 Geometrical properties

To find the solution of (19), (20), an understanding of the influence of the defects on the components of the metric $g_{\mu\nu}$ is needed. It is characterised by the Frank index ν which depends on the number of defects.

The gauge fields ω_μ, a_μ in (1) are a consequence of the curvature of the molecule and of the geometrical arrangement of the C-atoms in the molecule, respectively. Without these gauge fields, the Hamiltonian in (1) would have the form:

$$H_0 = i\gamma^\alpha e^\mu_\alpha [\partial_\mu - iA_\mu] \tag{21}$$

and the corresponding wave function we denote ψ_0. Then:

$$\psi(r, \varphi) = \exp(i\Omega_1(r, \varphi)) \exp(i\Omega_2(r, \varphi)) \psi_0(r, \varphi), \tag{22}$$

where Ω_1, Ω_2 are functions, their form following from the boundary conditions. Ω_1 stands for spin rotations, Ω_2 stands for frame rotations. Because:

$$H_0 \psi_0 = E\psi_0 \tag{23}$$

and, at the same time:

$$H\psi = E\psi, \tag{24}$$

it follows that:

$$H = \exp(i\Omega_1) \exp(i\Omega_2) H_0 \exp(-i\Omega_2) \exp(-i\Omega_1). \tag{25}$$

Then [8] a_μ, ω_μ have the form:

$$a_\mu = i \exp(i\Omega_1) \partial_\mu \exp(-i\Omega_1) = \partial_\mu \Omega_1, \tag{26}$$

$$\omega_\mu = -i \exp(i\Omega_2) \partial_\mu \exp(-i\Omega_2) = -\partial_\mu \Omega_2. \tag{27}$$

A more detailed derivation of Ω_1, Ω_2 can be found in [8,14]. Because this work is more oriented on the geometrical structure, we will not follow up the derivation of the form of a_μ, and the form of ω_μ presented in (15), (16) will be used.

It is possible to try to approximate the considered geometry by the metric of the cone [8]. However, this approach does not correspond to the real situation because of the point-like apex. Here we propose a method to avoid this problem.

3.1 Heptagonal defects

In the case of negative curvature and associated heptagonal defects, the parametrisation (8) for the case of the hyperboloid is:

$$(\xi, \varphi) \rightarrow (a\cosh\xi\cos\varphi, a\cosh\xi\sin\varphi, c\sinh\xi), \qquad (28)$$

where a and c are some dimensionless parameters. The corresponding diagonal components of the metric are:

$$g_{\xi\xi} = a^2\sinh^2\xi + c^2\cosh^2\xi, \qquad g_{\varphi\varphi} = a^2\cosh^2\xi \quad (29)$$

and the nonzero spin connection term:

$$\omega_\varphi^{12} = 1 - \frac{a\sinh\xi}{\sqrt{g_{\xi\xi}}}. \qquad (30)$$

The defect arises by the so-called cut and glue procedure – we cut a line in the graphene plane, add a 60° area and glue the resulting borders [8]. The geometrical properties of the new surface can be described with the help of the gauge potentials $\overrightarrow{W}_\mu^{(0)}$, which change the initial components of the metric (now denoted $g_{\mu\nu}^{(0)}$) [15]:

$$g_{\mu\nu}^{(0)} \rightarrow g_{\mu\nu} = \nabla_\mu \overrightarrow{R}_{(0)} \cdot \nabla_\nu \overrightarrow{R}_{(0)}, \qquad (31)$$

where:

$$\nabla_\mu \overrightarrow{R}_{(0)} = \partial_\mu \overrightarrow{R}_{(0)} + \left[\overrightarrow{W}_\mu^{(0)}, \overrightarrow{R}_{(0)}\right]. \qquad (32)$$

Then

$$\begin{aligned} g_{\mu\nu} = {} & \partial_\mu \overrightarrow{R}_{(0)} \cdot \partial_\nu \overrightarrow{R}_{(0)} + \partial_\mu \overrightarrow{R}_{(0)} \left[\overrightarrow{W}_\nu^{(0)}, \overrightarrow{R}_{(0)}\right] \\ & + \partial_\nu \overrightarrow{R}_{(0)} \left[\overrightarrow{W}_\mu^{(0)}, \overrightarrow{R}_{(0)}\right] + \left(\overrightarrow{W}_\mu^{(0)} \overrightarrow{W}_\nu^{(0)}\right) \overrightarrow{R}_{(0)}^2 \\ & - \left(\overrightarrow{W}_\mu^{(0)} \overrightarrow{R}_{(0)}\right) \left(\overrightarrow{W}_\nu^{(0)} \overrightarrow{R}_{(0)}\right) \end{aligned} \qquad (33)$$

and the components of the metric and the spin connection term will be changed such that:

$$g_{\xi\xi} = a^2\sinh^2\xi + c^2\cosh^2\xi, \qquad g_{\varphi\varphi} = a^2\alpha^2\cosh^2\xi, \quad (34)$$

$$\omega_\varphi^{12} = 1 - \frac{a\alpha\sinh\xi}{\sqrt{g_{\xi\xi}}}, \qquad \alpha = 1 + \nu, \qquad (35)$$

where $\nu = N/6$ is called the Frank index and N is the number of heptagons in the defect. In this paper, we take $N = 1$. Let us stress that as the number of defects increases, the geometrical structure becomes more complicated and we have to take into account additional assumptions [8,16].

We can encircle the origin of the defect ($\xi = 0$) by a closed loop C_ϵ and integrate over it. The result is:

$$\oint_{C_\epsilon} d\overrightarrow{s} = 2\pi\nu. \qquad (36)$$

No transformation of variables can change this value. If the values of the gauge field $\overrightarrow{W}_\mu^{(0)}$ are:

$$W_\mu^{(0)i=1,2} = 0, \qquad W_\mu^{(0)i=3} = W_\mu^{(0)}, \qquad (37)$$

where:

$$W_x^{(0)} = -\nu y/r^2, \qquad W_y^{(0)} = \nu x/r^2, \qquad r = \sqrt{x^2+y^2}, \qquad (38)$$

then:

$$\oint_{C_\epsilon} d\overrightarrow{s} = 2\pi\nu = \oint_{C_\epsilon} W_\mu^{(0)} dx^\mu, \qquad (39)$$

so $\overrightarrow{W}_\mu^{(0)}$ serves as a vortex-like potential with a nonzero flux. This flux should be eliminated by the corresponding integral over the spin connection, so we must get:

$$\lim_{\epsilon\rightarrow 0} \oint_{C_\epsilon} \omega_\varphi^{12} d\varphi = -2\pi\nu. \qquad (40)$$

Substituting (35) into the appropriate integral, the required result is readily obtained.

For our purpose, the gauge field $a_\varphi = N/4$. In the general case, a_φ depends on two constants N and M as $a_\varphi = N/4 + M/3$, where $M = -1, 0, 1$ for an even number of defects and $M = 0$ for an odd number of defects [8,10,12].

If the magnetic field is chosen in such a way that $\overrightarrow{A} = B(y, -x, 0)/2$, then:

$$A_\varphi = -\Phi\cosh^2\xi, \qquad A_\xi = 0, \qquad (41)$$

where:

$$\Phi = \frac{1}{2}a^2\Phi_0 B, \qquad \Phi_0 = \frac{e}{\hbar c}. \qquad (42)$$

The geometric units are used, i.e. $e = \hbar = c = 1$.

3.2 Pentagonal defects

The case of positive curvature is described in more detail in [10]. The parametrisation is changed into:

$$(\xi, \varphi) \rightarrow (a\sinh\xi\cos\varphi, a\sinh\xi\sin\varphi, c\cosh\xi), \qquad (43)$$

and the diagonal components of the metric are:

$$g_{\xi\xi} = a^2\cosh^2\xi + c^2\sinh^2\xi, \qquad g_{\varphi\varphi} = a^2\sinh^2\xi. \quad (44)$$

Introducing the gauge potentials $\overrightarrow{W}_\mu^{(0)}$ as for the heptagonal defects, the component $g_{\varphi\varphi}$ of the metric changes such that:

$$g_{\varphi\varphi} = a^2\alpha^2\sinh^2\xi, \qquad (45)$$

where $\alpha = 1 - \nu$. This means that in the cut and glue procedure, we cut a 60° area instead of inserting it. Then the nonzero spin connection term is:

$$\omega_{\varphi}^{12} = 1 - \frac{a\alpha \cosh\xi}{\sqrt{g_{\xi\xi}}}. \tag{46}$$

The values of the gauge field and the magnetic field are the same as in the previous case:

$$a_{\varphi} = N/4, \qquad \overrightarrow{A} = B(y, -x, 0)/2, \tag{47}$$

so that for the chosen parametrisation:

$$A_{\varphi} = -\Phi \sinh^2\xi, \qquad A_{\xi} = 0, \tag{48}$$

where Φ is defined as in (42).

4 Curvature

The Gaussian curvature is defined as:

$$K = \frac{(\partial_{xx}f)(\partial_{yy}f) - (\partial_{xy}f)^2}{(1 + (\partial_x f)^2 + (\partial_y f)^2)^2}, \tag{49}$$

where f means the z coordinate in (8) expressed with the help of x and y, i.e. formally we take $f(x, y) = z(\xi, \varphi)$. According to our presumptions, this quantity should be negative for heptagonal defects and positive for pentagonal defects.

4.1 Heptagonal defects

From a comparison of (8) and (28) it follows that:

$$\frac{x^2 + y^2}{a^2} - \frac{f(x, y)^2}{c^2} = 1, \tag{50}$$

so that:

$$f(x, y) = \frac{c}{a}\sqrt{x^2 + y^2 - a^2} = \frac{c}{a}\sqrt{r^2 - a^2}. \tag{51}$$

After calculationg the derivatives $\partial_{xx}f$, $\partial_{yy}f$ and $\partial_{xy}f$ we get:

$$K = -\frac{c^2}{(r^2(1 + \eta) - a^2)^2}, \tag{52}$$

where we use the definition of η given in (58). It is clear from this expression that the Gaussian curvature is negative for arbitrary values of r.

4.2 Pentagonal defects

For the parametrisation (43), we get:

$$\frac{f(x, y)^2}{c^2} - \frac{x^2 + y^2}{a^2} = 1, \tag{53}$$

so that:

$$f(x, y) = \frac{c}{a}\sqrt{x^2 + y^2 + a^2} = \frac{c}{a}\sqrt{r^2 + a^2}. \tag{54}$$

Calculating the required derivatives and substituting them into (49) yields:

$$K = \frac{c^2}{(r^2(1 + \eta) + a^2)^2}, \tag{55}$$

which shows that the Gaussian curvature is strictly positive in the case of pentagonal defects.

5 Solution of the Dirac equation

The solution of (19), (20) for heptagonal and pentagonal defects in the case of hyperboloidal geometry is introduced and the local density of states is calculated here. The linear elasticity theory [15,17] is used. For the numerical calculations of LDoS, the method described in [18] is exploited.

5.1 Heptagonal defects

The form of (19), (20) will be:

$$\partial_{\xi}\widetilde{u} - (\widetilde{j} - \widetilde{\Phi}\cosh^2\xi)\sqrt{\tanh^2\xi + \eta}\widetilde{u} = E\sqrt{g_{\xi\xi}}\widetilde{v}, \tag{56}$$

$$-\partial_{\xi}\widetilde{v} - (\widetilde{j} - \widetilde{\Phi}\cosh^2\xi)\sqrt{\tanh^2\xi + \eta}\widetilde{v} = E\sqrt{g_{\xi\xi}}\widetilde{u}, \tag{57}$$

where:

$$\widetilde{j} = (j + 1/2 - a_{\varphi})/\alpha, \qquad \widetilde{\Phi} = \Phi/\alpha, \qquad \eta = c^2/a^2. \tag{58}$$

The parameter $\eta \ll 1$ is a dimensionless parameter which describes the elasticity properties of the initial graphene plane. Due to these properties, the defects can be interpreted as small perturbations in the graphene plane. In the case of finite elasticity, we can use an approximation $\eta \sim \sqrt{\nu\epsilon}$, where $\epsilon \leq 0.1$ [10]. In this way, the elasticity is described by a small parameter ϵ. Its value is usually taken between 0.01 and 0.1. If we perform some necessary corrections to the gauge field ω_{μ}, then as we take $\epsilon \to 0$ we obtain the metric of the cone.

Let us now suppose $E = 0$. This energy corresponds to the so-called zero-energy mode which is appropriate for the electron states at the Fermi level. Then, the solution of (56), (57) is:

$$\widetilde{u}_0(\xi) = C(\triangle(\xi) + k\sinh\xi)^{k\widetilde{j} - \frac{\eta\widetilde{\Phi}}{2k}} \left(\frac{\cosh\xi}{\triangle(\xi) + \sinh\xi}\right)^{\widetilde{j}} \times \exp\left(-\frac{\widetilde{\Phi}\triangle(\xi)\sinh\xi}{2}\right), \tag{59}$$

$$\widetilde{v}_0(\xi) = C'(\triangle(\xi) + k\sinh\xi)^{-k\widetilde{j} + \frac{\eta\widetilde{\Phi}}{2k}} \left(\frac{\cosh\xi}{\triangle(\xi) + \sinh\xi}\right)^{-\widetilde{j}} \times \exp\left(\frac{\widetilde{\Phi}\triangle(\xi)\sinh\xi}{2}\right), \tag{60}$$

where:

$$k = \sqrt{1+\eta}, \qquad \triangle(\xi) = \sqrt{k^2\cosh^2\xi - 1}, \tag{61}$$

and C, C' are the normalisation constants.

For nonzero values of E the solution can be written as in [18]:

$$\widetilde{u}(\xi) = \widetilde{u}_0(\xi)\mathcal{U}(\xi), \qquad \widetilde{v}(\xi) = \widetilde{v}_0(\xi)\mathcal{V}(\xi), \tag{62}$$

where:

$$\mathcal{U}(\xi) = \mathcal{U}^{(0)}(\xi) + \varepsilon\mathcal{U}^{(1)}(\xi) + \cdots + \varepsilon^n\mathcal{U}^{(n)}(\xi) \tag{63}$$

and:

$$\mathcal{V}(\xi) = \mathcal{V}^{(0)}(\xi) + \varepsilon\mathcal{V}^{(1)}(\xi) + \cdots + \varepsilon^n\mathcal{V}^{(n)}(\xi), \tag{64}$$

$\varepsilon = \frac{Ea}{\hbar v_F}$ and we take $\hbar = v_F = 1$. Here n is an integer number and it is chosen according to the required precision. After substituting this approximation into (56) and (57) we get:

$$\partial_\xi\mathcal{U} = \varepsilon\triangle(\xi)\mathcal{V}\frac{\widetilde{v}_0}{\widetilde{u}_0}, \qquad \partial_\xi\mathcal{V} = -\varepsilon\triangle(\xi)\mathcal{U}\frac{\widetilde{u}_0}{\widetilde{v}_0}. \tag{65}$$

Putting $\mathcal{U}^{(0)} = 1$, $\mathcal{V}^{(0)} = 0$ and $i = 0, 1, \ldots, n-1$, the solution can be found numerically to be:

$$\mathcal{U}^{(i+1)}(\xi) = \int_0^\xi \mathcal{V}^{(i)}(\zeta)\Delta(\zeta)\frac{\widetilde{v}_0(\zeta)}{\widetilde{u}_0(\zeta)}d\zeta, \tag{66}$$

$$\mathcal{V}^{(i+1)}(\xi) = -\int_0^\xi \mathcal{U}^{(i)}(\zeta)\Delta(\zeta)\frac{\widetilde{u}_0(\zeta)}{\widetilde{v}_0(\zeta)}d\zeta. \tag{67}$$

For a given ξ_0, the local density of states is defined as:

$$LDoS(E) = \widetilde{u}^2(E,\xi_0) + \widetilde{v}^2(E,\xi_0). \tag{68}$$

To evaluate the local density of states, we have to calculate the normalisation constants C,C'. They differ for different values of E. For unnormalised solutions $\widetilde{u}'(\xi), \widetilde{v}'(\xi)$ of (56), (57) and each value of energy:

$$1/C^2 = 1/C'^2 = \int_0^{\xi_{max}} (\widetilde{u}'(\xi)^2 + \widetilde{v}'(\xi)^2)d\xi. \tag{69}$$

Since for $\xi_{max} = \infty$ the integral diverges, some finite value of ξ_{max} in some interval which is of particular interest is needed. In this work, we take $\xi_{max} = 2.5$ and $\xi_{max} = 2$. It follows from the parametrisation (28) that for the given values of ξ, the corresponding distance is $r = a\cosh\xi$, which means that for $a = 1$ Å we have $r_{max} = 6.13$ Å, or $r_{max} = 3.76$ Å. These values are of the same order as the size of the Brillouin zone which is formed by the single hexagons. Each atom in the hexagon lies at a distance 1.42 Å from its nearest neighbours [19,20]. This is the main principle of the tight-binding approximation [21] in which we only account for the influence of the nearest neighbours.

5.2 Pentagonal defects

The form of (19), (20) is:

$$\partial_\xi\widetilde{u} - (\widetilde{j} - \widetilde{\Phi}\sinh^2\xi)\sqrt{\coth^2\xi + \eta}\widetilde{u} = E\sqrt{g_{\xi\xi}}\widetilde{v}, \tag{70}$$

$$-\partial_\xi\widetilde{v} - (\widetilde{j} - \widetilde{\Phi}\sinh^2\xi)\sqrt{\coth^2\xi + \eta}\widetilde{v} = E\sqrt{g_{\xi\xi}}\widetilde{u}. \tag{71}$$

In the case $E = 0$, the corresponding solution is:

$$\widetilde{u}_0(\xi) = C(\triangle(\xi) + k\cosh\xi)^{k\widetilde{j}+\frac{\eta\widetilde{\Phi}}{2k}}\left(\frac{\sinh\xi}{\triangle(\xi)+\cosh\xi}\right)^{\widetilde{j}} \times \exp\left(-\frac{\widetilde{\Phi}\triangle(\xi)\cosh\xi}{2}\right), \tag{72}$$

$$\widetilde{v}_0(\xi) = C'(\triangle(\xi) + k\cosh\xi)^{-k\widetilde{j}-\frac{\eta\widetilde{\Phi}}{2k}}\left(\frac{\sinh\xi}{\triangle(\xi)+\cosh\xi}\right)^{-\widetilde{j}} \times \exp\left(\frac{\widetilde{\Phi}\triangle(\xi)\cosh\xi}{2}\right), \tag{73}$$

where:

$$k = \sqrt{1+\eta}, \qquad \triangle(\xi) = \sqrt{k^2\sinh^2\xi + 1}. \tag{74}$$

To calculate the solution for nonzero values of E and the local density of states we use the same procedure as presented for the heptagonal defects.

5.3 Local density of states

In Figures 1–3, the LDoS as a function of energy E and the parameter ξ is presented for hyperboloidal surfaces with the defects formed by 1 polygon. In all of these figures, we set $j = 0$ in (58) and $\epsilon = 0.01$ in the expression for η. We can see the evidence that for increasing B or ξ_{max}, the LDoS is decreasing and the decrease is faster for the pentagonal defects. If we took larger ξ_{max}, the LDoS would go to zero with the exception of a small number of energies for which we would obtain plane waves. The larger values of ξ are, however, unphysical because of the limited interval of validity of the tight-binding approximation.

The values we chose enable us to compare the LDoS for both kinds of defects subject to a small perturbation, where the difference between both approximations is not too large. Here we chose $\epsilon = 0.01$, but there are no significant changes for the LDoS if we let ϵ to grow up to 0.1, as we can easily see from the graphs in Figures 4 and 5, where we compare the LDoS for different values of the magnetic field at a fixed distance for $\epsilon = 0.01$ and 0.1.

6 Landau states

In [8,10], the Landau states for the researched defects are calculated for the conical and hyperboloidal geometry for

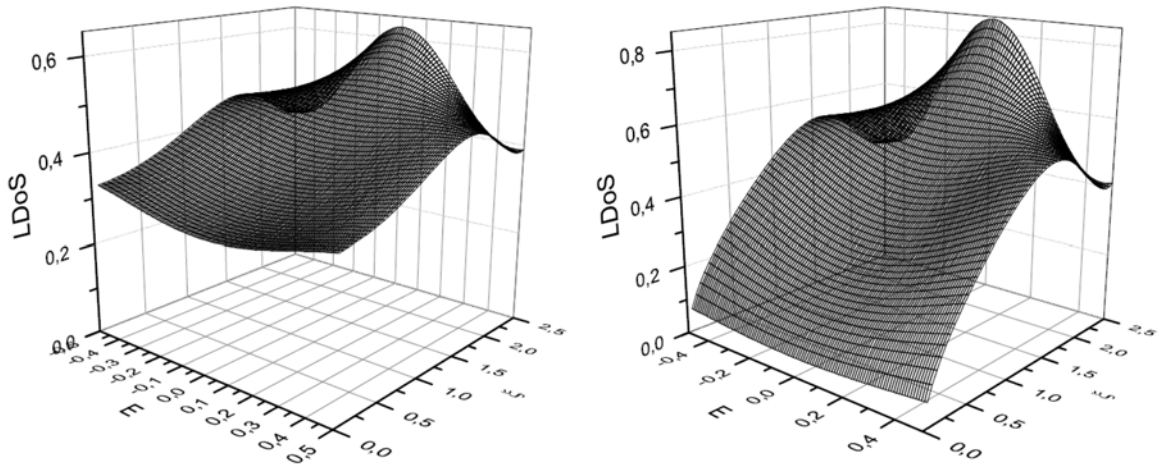

Fig. 1. LDoS as a function of $E \in (-0.5, 0.5)$ and $\xi \in (0, 2.5)$ for 1-heptagon defects (left part) and 1-pentagon defects (right part) for $B = 0$; $\epsilon = 0.01$.

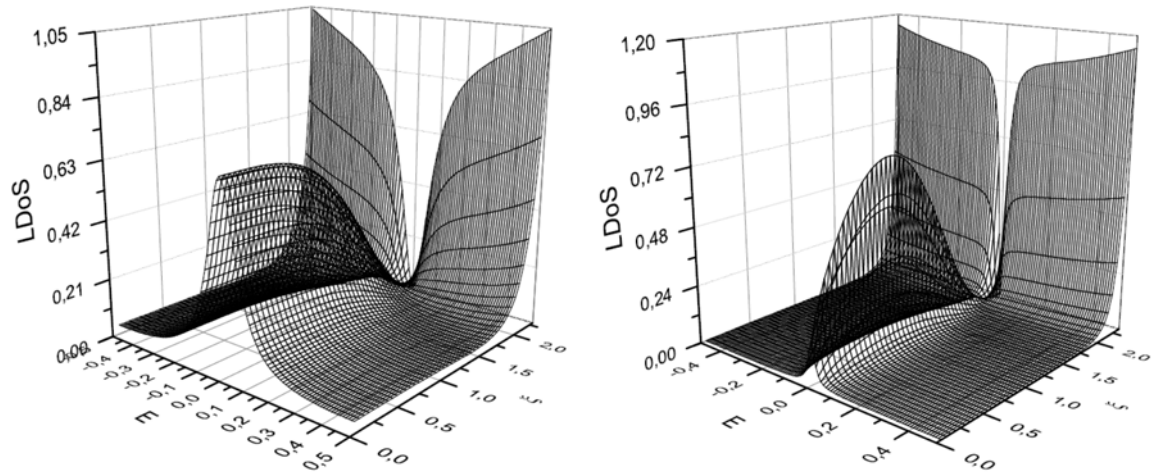

Fig. 2. LDoS as a function of $E \in (-0.5, 0.5)$ and $\xi \in (0, 2.5)$ for 1-heptagon defects (left part) and 1-pentagon defects (right part) for $B = 0.5$; $\epsilon = 0.01$.

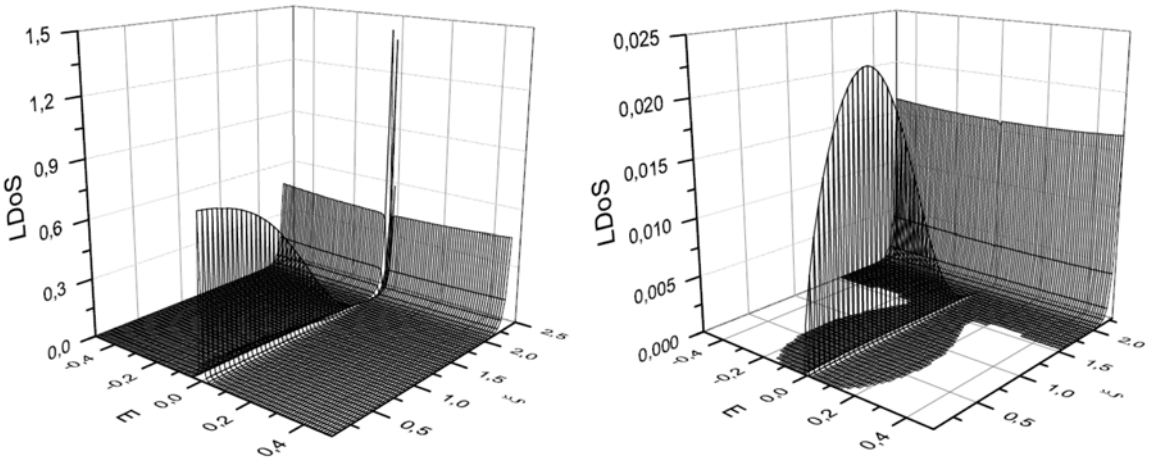

Fig. 3. LDoS as a function of $E \in (-0.5, 0.5)$ and $\xi \in (0, 2.5)$ for 1-heptagon defects (left part) and 1-pentagon defects (right part) for $B = 1$; $\epsilon = 0.01$.

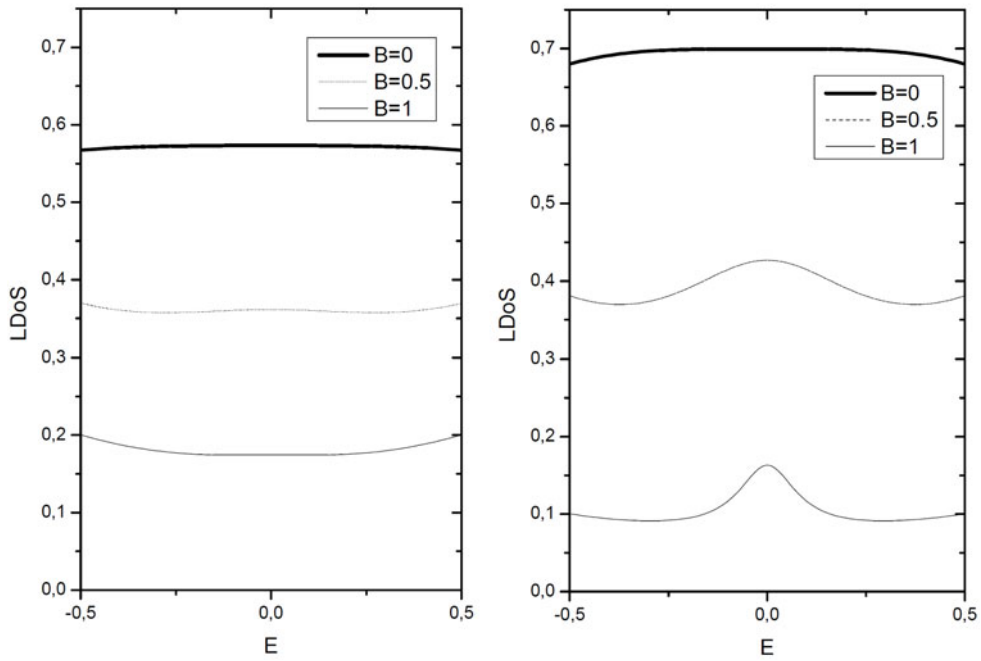

Fig. 4. LDoS as a function of $E \in (-0.5, 0.5)$ for 1-heptagon defects (left part) and 1-pentagon defects (right part); various values of B are used, $\xi = 1.5$, $\xi_{max} = 2$; $\epsilon = 0.01$.

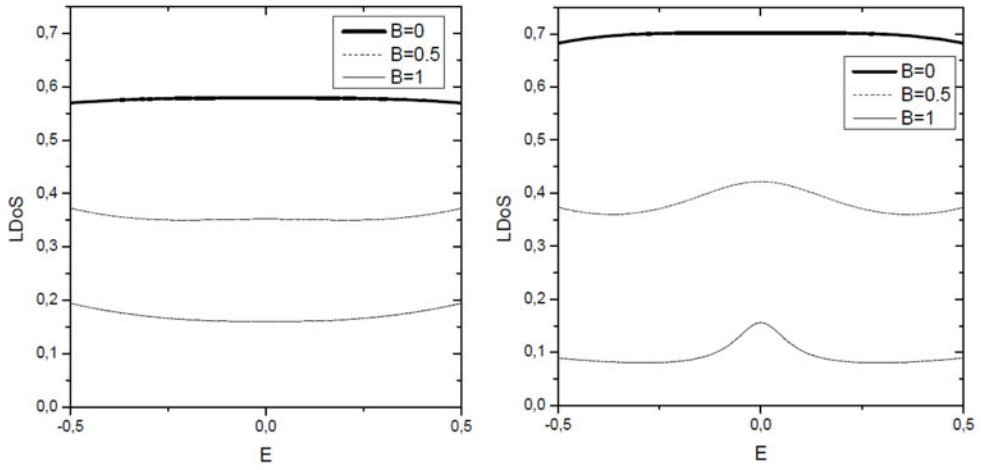

Fig. 5. LDoS as a function of $E \in (-0.5, 0.5)$ for 1-heptagon defects (left part) and 1-pentagon defects (right part); various values of B are used, $\xi = 1.5$, $\xi_{max} = 2$; $\epsilon = 0.1$.

positive curvature. In the case of conical geometry, where the corresponding parametrisation is:

$$(r, \varphi) \to (r\cos\varphi, r\sin\varphi, cr) \tag{75}$$

(c is an arbitrary constant) we have, according to [8], two kinds of Landau states. We use the first equation in (14) of [8] (1 defect) to define ν and distinguish the two cases.

The first case coincides with the Landau states of planar graphene [22]. It corresponds to $\nu \geq 0$ and we calculate the energy levels according to (22) in [8].

The second case coincides with $\nu \leq 0$, the energy levels are calculated according to (24) in [8] and the list of these Landau states for different values of the magnetic field is presented in Tables 1 and 2. In Tables 1 and 2, the "+" sign corresponds to the K point and the "−" sign corresponds to the K' point [14]. Because $j = -\frac{1}{2}$ corresponds [8] to $j = 0$ in (19), (20), we are looking for the corresponding energy levels.

Table 1. Landau states for pentagonal defects for $\nu \leq 0$, $|B| = 0.5$ and $j = -\frac{1}{2}$.

n	E_n
0	±0.89, ±1.18
1	±1.34, ±1.55
2	±1.67, ±1.84
3	±1.95, ±2.10

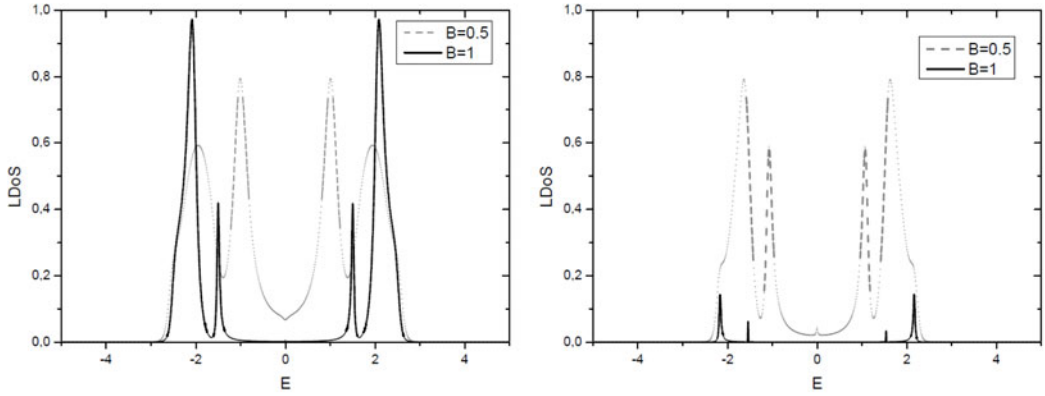

Fig. 6. Landau states for heptagonal (left part) and pentagonal defects (right part) for various values of B; $\xi_{max} = 2$, $\xi = 2$, $\epsilon = 0.01$.

Table 2. Landau states for pentagonal defects for $\nu \leq 0$, $|B| = 1$ and $j = -\frac{1}{2}$.

n	E_n
0	± 1.25, ± 1.66
1	± 1.89, ± 2.19
2	± 2.35, ± 2.59
3	± 2.75, ± 2.96

Let us compare the Landau states for the hyperboloidal geometry with the values calculated for a cone and graphene. For this purpose, we do an extension of the interval of energies for which we calculate the LDoS. The result is seen in Figure 6. We see that for pentagonal defects, the values ± 1.67 and ± 2.19 from Tables 1 and 2 can be found by this method. The reason for the presence or absence of other peaks could be the incompleteness of the list of Landau states for the hyperboloidal geometry and a low magnitude of some peaks. It is also possible that some of the Landau states characterising the conical and planar geometries do not appear in the case of the hyperboloidal geometry. For the negative curvature, the appropriate energy levels have similar positions but they are shifted to the left.

The comparison of our results with the Landau states as expected for multilayer graphene [23] is also interesting. These results differ in that for zero-energy states ($n = 0$, see [23]), there are nonzero Landau states with low magnitude. For higher n, the Landau states are calculated with the help of the approximation formula (22) in [23], where $\Gamma_B = \sqrt{\frac{3}{2}B}\gamma_0$, N is the number of graphene layers, $\gamma_0 = 3$, $\gamma_1 = 0.4$, $\gamma_2 = -0.02$ and the next parameters are substituted according to the notation in that article. As we can see in Tables 3–5, the results acquired using this formula are higher in order than the Landau states calculated in this paper for the hyperboloid geometry. Thus, the Landau states for multilayer graphene and for the hyperboloid geometry presented in this paper are completely different. The discrepancy may be explained by considering the influence of atoms in the neighbour and next-neighbour layers in the multilayer graphene which do not exist in the case of one-layer graphene.

Table 3. Landau states for 3-layer planar graphene.

n	E_n	
	$\|B\| = 0.5$	$\|B\| = 1$
0	± 16.87	± 33.75
1	± 29.23	± 58.46
2	± 41.33	± 82.67

Table 4. Landau states for 4-layer planar graphene.

n	E_n	
	$\|B\| = 0.5$	$\|B\| = 1$
0	± 14.75	± 29.50
1	± 25.55	± 51.10
2	± 36.13	± 72.26

Table 5. Landau states for 5-layer planar graphene.

n	E_n	
	$\|B\| = 0.5$	$\|B\| = 1$
0	± 13.78	± 27.56
1	± 23.87	± 47.73
2	± 33.75	± 67.50

6.1 Influence of Zeeman effect

The aim of this paper is to investigate the geometrical properties and related gauge fields in the vicinity of the heptagonal defects in a graphene layer. However we could extend our research and consider, for example, the influence of the Zeeman effect. In this case, the Landau states would be degenerate. For a graphene layer, the degeneration of the nth Landau state is described in [24]. The spectrum then coincides with multiples of the eigenvalues of the number operators, i.e. $\sqrt{2B}\sqrt{n}$, $\sqrt{2B}\sqrt{n+1}$ and $-\sqrt{2B}\sqrt{n}$, $-\sqrt{2B}\sqrt{n+1}$, resp. for the K point, K' point, respectively,where $n = 0, 1, 2, \ldots$ For higher values of n,

Table 6. Shift of Landau states for pentagonal defects for $\nu \leq 0$, $|B| = 0.5$ and $j = -\frac{1}{2}$.

n	E_n	
	1. spin state	2. spin state
0	± 0.89, ± 1.18	± 1.34, ± 1.55
1	± 1.34, ± 1.55	± 1.67, ± 1.84
2	± 1.67, ± 1.84	± 1.95, ± 2.10
3	± 1.95, ± 2.10	± 2.20, ± 2.32

Table 7. Shift of Landau states for pentagonal defects for $\nu \leq 0$, $|B| = 1$ and $j = -\frac{1}{2}$.

n	E_n	
	1. spin state	2. spin state
0	± 1.25, ± 1.66	± 1.89, ± 2.19
1	± 1.89, ± 2.19	± 2.35, ± 2.59
2	± 2.35, ± 2.59	± 2.75, ± 2.96
3	± 2.75, ± 2.96	± 3.10, ± 3.29

the difference would be small, so it is useful to neglect this effect in our calculations. Let us review the shift of the Landau states in all of the cases presented above.

We have already described the situation for graphene. Let us stress that in case of zero-energy modes, i.e. $n = 0$, for the nonzero magnetic field the Landau state would also be doubly- degenerate and the corresponding eigenvalues would be 0, $\sqrt{2B}$, respectively.

Let us now reformulate the formula (24) in [8] for the case when the aforementioned parameter $\nu \leq 0$. In accordance with the calculation of the Landau state shift in graphene, we suppose that for the nth Landau state, the shift would be represented by two states which we obtain by the substitution of the values n and $n+1$ into the corresponding formula. So, the resulting values will be similar to those presented in Tables 1 and 2. They are presented in Tables 6 and 7 for comparison. The difference of the presented splitted states is approximately the same as in the graphene layer [22]. For higher values of n, this difference vanishes.

The shift of the Landau states for the multilayer graphene is described in [24].

The case of the curved surface which arises as the result of a small perturbation is more complicated. For fullerene, for example, the calculation of the Landau states and their shift can be seen in [25]. For a negatively curved hyperboloid, we would construct, in analogy with [10], a perturbation to the Dirac operator on the surface of a cone. According to (1), (56) and (57), the Dirac operator for a negatively curved hyperboloid is:

$$\begin{aligned}\mathcal{D} &= -\sigma_2\frac{\partial_\xi}{\sqrt{g_{\xi\xi}}} + \sigma_1\frac{\partial_\varphi}{\sqrt{g_{\varphi\varphi}}} + \frac{\sigma_2}{\sqrt{g_{\varphi\varphi}}}\left(\frac{1}{2}\omega - a_\varphi - A_\varphi\right)\\ &= -\sigma_2\frac{\partial_\xi}{\sqrt{g_{\xi\xi}}} + \sigma_1\frac{\partial_\varphi}{\sqrt{g_{\varphi\varphi}}} + \frac{\sigma_2}{\sqrt{g_{\varphi\varphi}}}\\ &\quad\times\left(\frac{1}{2} - \frac{a\alpha\sinh\xi}{2\sqrt{g_{\xi\xi}}} - a_\varphi - A_\varphi\right).\end{aligned} \tag{76}$$

Because:

$$\begin{aligned}g_{\xi\xi} &= a^2\sinh^2\xi + c^2\cosh^2\xi = a^2\sinh^2\xi(1+\eta\coth^2\xi),\\ g_{\varphi\varphi} &= a^2\alpha^2\cosh^2\xi,\end{aligned} \tag{77}$$

we can write, for small η:

$$\begin{aligned}\frac{1}{\sqrt{g_{\xi\xi}}} &= \frac{1}{a\sinh\xi\sqrt{1+\eta\coth^2\xi}}\\ &\sim \frac{1}{a\sinh\xi}\left(1 - \frac{1}{2}\eta\coth^2\xi\right),\end{aligned} \tag{78}$$

and the Dirac operator becomes:

$$\begin{aligned}\mathcal{D} &= -\sigma_2\frac{\partial_\xi}{a\sinh\xi} + \sigma_1\frac{\partial_\varphi}{a\alpha\cosh\varphi}\\ &\quad + \frac{\sigma_2}{a\alpha\cosh\xi}\left(\frac{1-\alpha}{2} - a_\varphi - A_\varphi\right)\\ &\quad + \eta\sigma_2\frac{\cosh^2\xi}{2a\sinh^2\xi}\left(\frac{\partial_\xi}{\sinh\xi} + \frac{1}{\cosh\xi}\right)\\ &= D_0 + \eta D_1.\end{aligned} \tag{79}$$

Because we do not know the exact values of the Landau states for a hyperboloidal surface, the appropriate calculations can not be performed. Otherwise, the procedure would be the same as in [25].

7 Conclusion

We have studied the electronic structure of disclinated graphene in the vicinity of heptagonal and pentagonal defects depending on the kind of a curvature (negative or positive). Hyperboloidal parametrisations (28), (43) were assumed after rejection of the conical metric. The continuum field-theory gauge model was used, in which the disclinations are incorporated using the vortex-like potential (37), (38) for the calculation of the components of the metric. The arising fictitious flux was compensated for by the gauge flux of spin connection field (15), (16). The potential (37), (38) also results in the dependence of the corresponding Dirac equation on the Frank index α which includes the number of defects. The defects are involved in (58) with the help of the parameter ϵ, which comes from the elasticity properties of the graphene.

Next, we incorporated a uniform magnetic field (41), (48) that can significantly influence the LDoS. These were calculated from the solution of the Dirac equation, which we obtained numerically with the help of the extension of an analytical solution for zero-energy modes (59), (60), (72), (73).

In all the presented figures, the behaviour of the LDoS is compared for both kinds of defects. For very small values of ϵ, this behaviour is similar for both kinds of defects, but

it is more spread for heptagonal defects. We have found that varying the value of ϵ does not significantly affect LDoS. We also compared the resulting Landau states with the theoretical prediction coming from the corresponding values for a graphene plane and conical metric. We see that the different geometrical structures influence the position of the Landau states. Further influence comes from the presence of the Zeeman couplings. They are not related to the geometrical structure of defects, but we can see in Tables 6 and 7 that the different splittings of the energy levels in the n-th Landau state is non-negligible and we will study this further in future research.

To conclude, the presented results have a large potential use for calculating the metallic properties of carbon nanohorns which have widespread application in electronic devices. Let us mention the significance of the zero-energy modes. Generally, they appear as a solution for disclinated graphene in the presence of a magnetic field [26] and they play a key role in explanations of anomalies, paramagnetism, high-temperature superconductance etc.

We have to stress that we assumed defects in which only 1 heptagon or 1 pentagon appeared. For a higher number of polygons in defects the calculation is more complicated, especially for heptagons, because in contrast to pentagonal defects problems with the geometrical interpretation occur. It will be useful to perform calculations for more complicated forms of defects in the future.

We sincerely thank Prof. V.A. Osipov for his helpful comments and advice. The work was supported by the Slovak Academy of Sciences in the framework of CEX NANOFLUID, by the Science and Technology Assistance Agency under Contract No. APVV 0509-07, 0171 10, VEGA Grant No. 2/0069/10 and by the Ministry of Education Agency for Structural Funds of EU in the frame of project 26220120021.

References

1. H.W. Kroto et al., Nature **318**, 162 (1985)
2. H. Kroto, Rev. Mod. Phys. **69**, 703 (1997)
3. V.A. Osipov, Phys. Lett. A **164**, 327 (1992)
4. H. Ajiki, T. Ando, J. Phys. Soc. Jpn **64**, 4382 (1995)
5. T. Yaguchi, T. Ando, J. Phys. Soc. Jpn **70**, 3641 (2001)
6. R. Saito, G. Dresselhaus, M.S. Dresselhaus, Phys. Rev. B **53**, 2044 (1996)
7. T. Ando, J. Phys. Soc. Jpn **74**, 777 (2005)
8. P.E. Lammert, V.H. Crespi, Phys. Rev. B **69**, 035406 (2004)
9. C. Chuang, B.-Y. Jin, J. Chem. Inf. Model. **49**, 1664 (2009)
10. E.A. Kochetov, V.A. Osipov, R. Pincak, J. Phys.: Condens. Matter **22**, 395502 (2010)
11. V.A. Osipov, E.A. Kochetov, M. Pudlak, J. Exp. Theor. Phys. **96**, 140 (2003)
12. D.V. Kolesnikov, V.A. Osipov, Eur. Phys. J. B **49**, 465 (2006)
13. E.A. Kochetov, V.A. Osipov, JETP Lett. **91**, 110 (2010)
14. Yu. A. Sitenko, N.D. Vlasii, Nucl. Phys. B **787**, 241 (2007)
15. E.A. Kochetov, V.A. Osipov, J. Phys. A **32**, 1961, (1999)
16. S. Berber, Y.-K. Kwon, D. Tomanek, Phys. Rev. B **62**, R2291 (2000)
17. H.S. Seung, D.R. Nelson, Phys. Rev. A **38**, 1005, (1988)
18. D.V. Kolesnikov, V.A. Osipov, JETP Lett. **79**, 532 (2004)
19. P.R. Wallace, Phys. Rev. **71**, 622 (1947)
20. J.C. Slonczewski, P.R. Weiss, Phys. Rev. **109**, 272 (1958)
21. J. Gonzalez, F. Guinea, M.A.H. Vozmediano, Nucl. Phys. B **406**, 771 (1993)
22. J.W. McClure, Phys. Rev. **104**, 666 (1956)
23. M. Koshino, E. McCann, Phys. Rev. B **83**, 165443 (2011)
24. M. Ezawa, J. Phys. Soc. Jpn **76**, 094701 (2007)
25. R. Pincak, M. Pudlak, in *Progress in Fullerene Research*, edited by F. Columbus (Nova Science Publishers, New York, 2007)
26. R. Jackiw, Phys. Rev. D **29**, 2375 (1984)